



Mechanical Properties and Energy Evolution of Red Sandstone Under the Influence of Acid Corrosion

Yongsheng Liu¹ · Wang Liu¹ · Cui Wang² · Maolin Zhai¹

Received: 5 November 2023 / Accepted: 19 February 2024 / Published online: 20 March 2024
© King Fahd University of Petroleum & Minerals 2024

Abstract

This study aimed to investigate the effects of acid corrosion on mechanical properties and fractal characteristics of red sandstone. The mineral composition of red sandstone was analyzed using X-ray diffraction. The mechanical properties and acoustic emission (AE) signals of red sandstone specimens corroded by sulfuric acid solution with pH values of 1, 3, and 5 for 30 days were determined by uniaxial compression test and AE technique. The energy dissipation law and the fractal damage characteristics of red sandstone specimens after acid corrosion were analyzed based on the energy and fractal theories. The results indicated that the compressive strength and elastic modulus of red sandstone specimens corroded by acid solution decreased. In addition, the peak strain increased, the cumulative AE ringing count decreased, and the duration of high-level AE ringing shortened. These phenomena became more pronounced as the acidity of the solution increased. The peak values of the total energy and the elastic strain energy of the acid-solution-corroded red sandstone specimens decreased. The energy absorption capacity and energy storage limit of rock specimens also decreased. The fractal dimension and the degree of fragmentation decreased with the dissipated energy used for fragmentation. This research provides valuable insights into the prevention and control of sub-surface geotechnical hazards in acid rain-prone areas.

Keywords Acid corrosion · Mechanical properties · Acoustic emission · Energy evolution · Fractal dimension

1 Introduction

With the increasing demand for geological resources, studying the mechanical properties and behavior of rocks has attracted great interest [1]. Red sandstone, a common sedimentary rock, is very valuable in a variety of fields such as energy development, underground engineering, and geological hazard management. Nonetheless, the execution of a project is greatly impacted by the existence of groundwater. In particular, groundwater is usually acidic due to the presence of chemical ions and is more acidic in areas where acid rain is frequent [2, 3]. Acid corrosion of the rock causes a progressive deterioration of its mechanical and physical qualities, or even its complete destruction [4, 5]. The variation of energy and strength during rock failure process is

related in some way, and this energy evolution law can accurately capture the nature of failure as well as the variation in rock strength under load [6, 7]. For this reason, understanding the mechanical properties and energy evolution laws of red sandstone under acid corrosion conditions is crucial to ensure the long-term viability of underground engineering.

The evolution mechanism of rock damage and the shifting patterns of mechanical properties resulting from chemical reactions have been the subject of extensive research in recent years. Huang et al. [8] examined the mechanical parameter deterioration patterns in limestone subjected to acid corrosion and analyzed the mechanism underlying the deterioration of acid-attacked limestone's strength. Cao et al. [9] studied the effect of chemical corrosion by water on the dynamic mechanical properties of rock by using the SHPB compression bar test system. Based on triaxial compression tests, Chen et al. [10] examined the changes in physical and mechanical parameters in red sandstone following corrosion by acid solutions with varying pH values. Li et al. [11] explored the effect of acid solution corrosion time on the physical and mechanical properties of sandstone, derived damage variables for acid-corroded sandstone, and

✉ Wang Liu
2020019081400003@ecjtu.edu.cn

¹ School of Civil Engineering and Architecture, East China Jiaotong University, Nanchang 330013, China

² Department of Civil Engineering, Jiangxi Institute of Construction, Nanchang 330200, China



quantitatively assessed the degree of damage. Huo et al. [12, 13] investigated the variations in peak strength, elastic modulus, and mass loss rate in sandstone following acid corrosion using uniaxial compression tests and CT scans. Bai et al. [14] investigated the corrosive effect of an acidic environment on red mud–fly ash cementitious materials, which offered theoretical support for the application of red mud–fly ash cementitious materials in complex stratigraphic environments. Zhang et al. [15] investigated the chemical weathering process of silicate rocks and analyzed the factors causing the formation of carbonate deposition from a chemical reaction perspective.

The mechanisms of rock corrosion in acidic environments are not well documented in the literature, so more research is still needed. The process of rock deformation and destruction involves the dissipation and the release of internal energy [16, 17]. The fractal dimension of a damaged rock provides a quantitative description of its damage [18, 19]. Wu et al. [20] investigated the evolution of the energy and the storage characteristics of red sandstone during the loading and destruction process. Meng et al. [21] examined the influence of confining pressure and temperature on the evolution of energy through triaxial cyclic loading and unloading tests on rock. Yang et al. [22] studied the relationship between energy dissipation and rock fragmentation degree by performing the impact compression test. Gong et al. [23] quantitatively studied the energy dissipation characteristics of rock materials during dynamic tensile damage by conducting a dynamic Brazilian disk test on red sandstone with the SHPB device. The fractal characteristics of rock fragmentation indicated the degree of rock fragmentation and the distribution of the size of the block, while the dissipated energy indicated the effective work of crushed rock. The energy dissipation law of the rock is directly related to the fractal characteristics of fragmentation [24–26]. Wang et al. [27] conducted experiments to test the energy dissipation density of the rock at various strain rates and analyzed the relationship between the fractal dimensions and the energy dissipation characteristics. Chai et al. [28] employed geometric and microscopic fractal methods to analyze the energy dissipation characteristics of rock cracks and studied the process of initiation, distribution, and expansion of rock cracks. Tian et al. [29] performed rock fracture simulation experiments on granite specimens and analyzed the fractal characteristics of the resulting fragments. The energy mechanism and fracture fractal features of rock damage have been greatly improved by these research findings, but little is known about the energy dissipation law and the fracture fractal features of rock under acid corrosion. Subsequent research in this field is therefore crucial and can offer insightful information for the prevention and control of underground geotechnical hazards in acid rain-prone areas.

This study examined the mechanical property degradation of red sandstone corroded by different acid solutions by

using uniaxial compression test, AE monitoring technique, and X-ray diffraction test. The change in the characteristic parameters of AE was analyzed, and the causes of the internal structure degradation of red sandstone from the standpoint of the corrosion mechanism were explored from the perspective of corrosion mechanism. The study also integrated energy dissipation theory and fractal theory to examine the energy dissipation law and the fragmentation fractal characteristics of red sandstone during the destruction process. The findings of the study offer a theoretical basis for hazard prevention and control in underground geotechnical engineering projects situated in acid rain-prone areas.

2 Test content and Program

2.1 Red Sandstone Preparation

The rock specimens used for the test were taken from Yunnan Province, China, which is known for its widespread red sandstone and high acid rain intensity. To ensure accurate test results and minimize sampling errors, all rock specimens were collected from the same rock mass. X-ray diffraction was used to test and analyze the mineral composition of these rock specimens. The major minerals found in these specimens included quartz, potassium feldspar, sodium feldspar, and calcite. The mineral content of the rock specimens is listed in Table 1.

The rock specimens were prepared with a two-step approach. Firstly, the rock block was crushed mechanically in the field. A 50-mm diameter cylinder was then drilled out of the rock block using a core drilling machine. A 100-mm high cylinder was then made from the core using a cutting machine. Following the guidelines of the International Society for Rock Mechanics (ISRM), the specimens were shaped into standard cylinders with a height of 100 mm and a diameter of 50 mm. To ensure accuracy and minimize errors, rock specimens were carefully selected from large rock masses that had no visible cracks. After coring, the specimens were subjected to a thorough inspection to exclude specimens with surface cracks or spalling. In addition, the specimens were carefully ground with a grinding machine, which ensured that the non-parallelism between the two end faces of the specimens was less than 0.02 mm and the non-perpendicularity between the end faces and the sides was also less than 0.02 mm.

2.2 Preparation of Acidic Solutions and Specimens Corrosion

The experiment used sulfuric acid, a key ingredient of acid rain, to simulate an acid environment. The aim was to study the degradation pattern of red sandstone under acidification

Table 1 Mineral content of rock specimens

Mineral content	Quartz	Potassium feldspar	Sodium feldspar	Calcite	Else
Percentage (%)	53.19	3.16	27.82	9.36	6.47



(a) Natural condition



(b) pH=1



(c) pH=3



(d) pH=5

Fig. 1 Red sandstone specimens under different corrosion conditions

conditions. Sulfuric acid solutions with pH values of 1, 3, and 5 were prepared by mixing distilled water and concentrated sulfuric acid in specific proportions. To ensure a complete reaction between the acidic solution and the specimens, the specimens were immersed in the solution and corroded for 30 days. Four groups of red sandstone specimens were prepared for the experiment. One group was kept under natural condition, while the remaining three groups were corroded in sulfuric acid solutions with pH values of 1, 3, and 5 for 30 days. The pH of the acid solution was monitored regularly with a pH test pen to maintain the preset pH. The pH of the solution was maintained by topping up the sulfuric acid solution. Figure 1 presents the red sandstone specimens under different corrosion conditions.

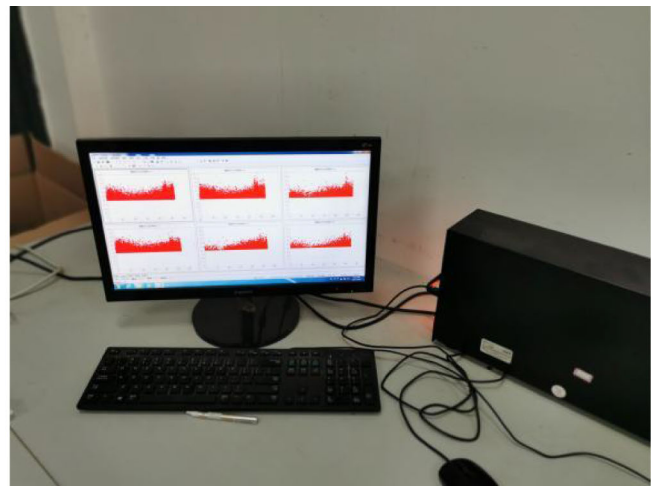
2.3 Test Equipment and Method

A displacement-controlled mode with a loading rate of 0.06 mm/min was used to conduct uniaxial loading tests using the ZTRE-210 microcomputer-controlled rock triaxial testing system. AE data were collected during the uniaxial compression of red sandstone specimens using a Micro-II Express Digital Acoustic Emission monitoring system. A fixed threshold of 40 dB and a sampling rate of 1 MHz were set for the system. The uniaxial loading system and the AE recording system are illustrated in Fig. 2.

A total of six sensors were employed in the experiment to improve signal acquisition and precisely localize acoustic emission events. These sensors were set up in two layers, with three sensors per layer positioned in the plane at 120°



(a) Uniaxial loading system



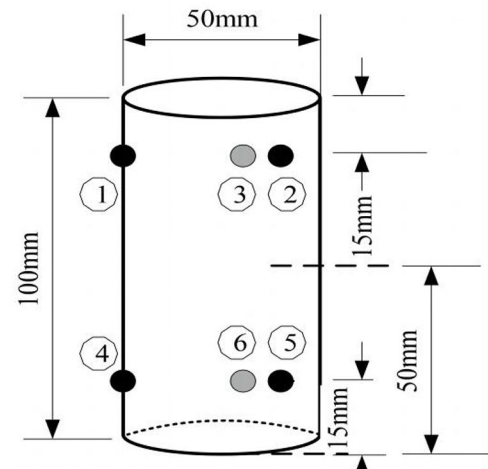
(b) Acoustic emission recording system

Fig. 2 Test equipment

Fig. 3 Rock specimens test diagram



(a) Rock acoustic emission tests



(b) Layout of the acoustic emission sensors

angles. The upper and lower sensors were positioned in a straight line, 15 mm away from the corresponding upper and lower end faces. Figure 3 displays sensor layouts for rock AE tests.

3 Test results and Analysis

3.1 Mechanical Character Analysis

Three rock specimens were chosen, and each underwent varying conditions of corrosion. The mechanical parameters of these specimens were determined through uniaxial compression tests, and the results are presented in Table 2. The rock specimen selected for further analysis was the one

whose compressive strength was closest to the average value among each group of specimens. As demonstrated in Table 2, the specimens under natural condition, pH = 5, pH = 3, and pH = 1 corrosion conditions were labeled as T-1, T-5, T-7, and T-12, respectively. The stress–strain curves are displayed in Fig. 4.

The test results indicated that the uniaxial compressive stress–strain curves of the specimens after corrosion under different acid solution conditions were similar to those under natural condition. These curves could be divided into three stages: compression stage, elastic stage, and plastic stage. In the compression stage, the stress–strain curves of the specimens under natural condition had a concave portion shorter than those of the specimens after corrosion in an acid environment. Moreover, the concave portion of the curve lengthened

Table 2 Mechanical parameters of the rock specimens

Corrosion conditions	Specimen number	Peak Strain ($\times 10^{-3}$)	Peak stress (MPa)	Elastic modulus (GPa)
Natural	T-1	3.31	70.89	28.98
	T-2	3.32	69.77	28.43
	T-3	3.28	72.03	29.72
pH = 5	T-4	3.70	51.78	18.76
	T-5	3.68	52.34	18.94
	T-6	3.61	53.08	19.81
pH = 3	T-7	3.94	38.96	13.67
	T-8	3.96	37.87	12.94
	T-9	3.89	39.66	13.79
pH = 1	T-10	4.17	33.67	12.07
	T-11	4.04	35.65	13.20
	T-12	4.12	34.43	12.50

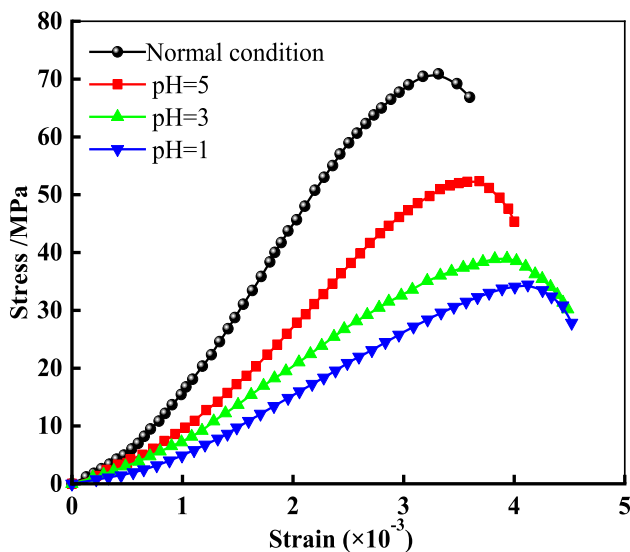


Fig. 4 Stress–strain curves of rock specimens under different corrosion conditions

with the increased acidity of the corrosive solution. Simultaneously, the slope of the stress–strain curve decreased as the acidity of the corrosive solution increased.

The relationship between stress, strain and elastic modulus of rock specimens under different corrosion conditions are displayed in Fig. 5. Further analysis revealed that the peak stresses of the specimens subjected to corrosion under different acid solution conditions (natural, pH = 5, pH = 3, and pH = 1) were 70.89, 52.34, 38.96, and 34.43 MPa, respectively. This corresponded to a discount rate of 26.17%, 45.04%, and 51.43% compared to the specimens under natural condition. Likewise, the elastic modulus of the specimens corroded by different acid solutions was 45.7, 37.8, 30.5, and 28.2 GPa, with discount rates of 34.64%, 52.83%, and 56.87%,

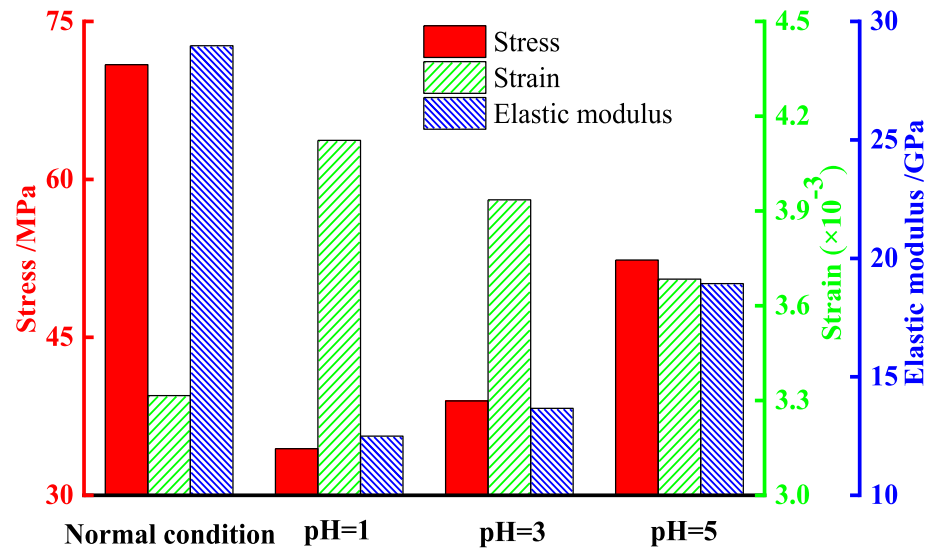
respectively. These findings indicated a gradual decrease in the compressive strength and elastic modulus of the rock specimens as the acidity of the corrosion solution increased. Furthermore, the peak strains of the specimens under natural condition, pH = 5, pH = 3, and pH = 1 acid solution corrosion conditions were 3.31×10^{-3} , 3.68×10^{-3} , 3.94×10^{-3} , and 4.12×10^{-3} , respectively. This suggested that the peak strains of the specimens increased with the increasing acidity of the corrosion solution.

Extensive analysis revealed that the mineral constituents of the red sandstone specimen underwent physical and chemical reactions with the acid solution. This led to the penetration of the solution into the internal pores of the specimen, forming a water film on the surface of the mineral particles. As a result, the bond between the mineral particles was weakened by the generation of pore water pressure. Furthermore, the minerals in the rock specimen also underwent a chemical reaction with the acid solution, which caused the minerals to dissolve and precipitate. Because of this, the elastic modulus and load-bearing capacity of rock specimen decreased, but its peak strain and plastic deformation capacity increased.

3.2 Characterization of Acoustic Emission

To study the development of internal microscopic defects and cracks in red sandstone corroded by various acid solutions, the intensity of AE events was quantitatively analyzed. This analysis involved capturing the AE ringing count and the cumulative AE count to assess the degree of damage to red sandstone under different corrosion conditions. The variation of the characteristic parameters of AE with various pH values of the corrosion solution during the deformation and damage process of the specimen are shown in Fig. 6. Notably, the AE ringing count in the compression and elastic stages was significantly lower than that in the plastic stage. Therefore, to

Fig. 5 Relationship between stress, strain and elastic modulus of rock specimens under different corrosion conditions



better describe the AE characteristics of each stage, the AE ringing counts in the compression and elastic stages were scaled-up with respect to time and were represented by the Zone I.

During the compression stage, the initial defects in the rock specimens were compacted and closed under load. The cumulative AE ring numbers at the end of the compression stage of the specimens were 7.5×10^4 , 1.4×10^5 , 1.7×10^5 , and 2.9×10^5 for the natural condition, pH = 5, pH = 3, and pH = 1 acid solution corrosion conditions, respectively. The cumulative ring number increased with increasing acidity of the corrosion solution. Examining the zoomed-in view of the AE ringing count in Zone I revealed that the specimens under natural conditions exhibited lower ringing counts during the compaction stage compared with those corroded by the acid solution. This difference was attributed to the chemical reaction between the internal mineral components of the rock specimens and the sulfuric acid solution during acid corrosion. This reaction led to the decomposition and precipitation of the mineral components, causing the defects inside the specimen to enlarge. These enlarged defects were then frictionally closed during the loading process, resulting in the strong AE signals. Furthermore, the AE signal became stronger as the acidity of the corrosion solution increased.

During the elastic deformation stage, the AE ringing count and cumulative ringing count of the specimens experienced a gradual increase in both under natural condition and corrosion with acid solutions. This was attributed to the closure of internal defects and the improved integrity of the rock specimens after the compression stage. This meant that crack development remained at a low level, leading to a lower AE ringing count.

During the loading process, the specimens underwent a plastic stage in which the AE ringing counts started to

increase. These counts remained at a high level until the specimen was destroyed, with the cumulative ringing counts rapidly increasing and peaking at the time of specimen destruction. The cumulative ringing counts for the specimens under different corrosion conditions were 13.87×10^6 , 11.55×10^6 , 9.95×10^6 , and 8.94×10^6 for natural, pH = 5, pH = 3, and pH = 1 corrosion conditions, respectively. As the acidity of the corrosion solution increased, the cumulative ringing counts decreased, and the duration of the high-level AE ringing counts also decreased. This suggested that corrosion deteriorated the internal structure of rock specimens, reducing the energy required for deformation and increasing their plasticity.

3.3 Analysis of Acid Corrosion Mechanism

Both the mineral composition and the nature of cement of the rocks affected their mechanical properties. The mechanical properties of red sandstone corroded by acid solutions deteriorated due to a complex process involving various physicochemical effects.

Certain voids were formed in the natural rock by physical action. A water film formed on the mineral particles as a result of the acid solution's entry into these voids. This water film increased the pressure of water inside the voids, reducing friction and contact between the mineral particles. On the other hand, as the chemical reaction proceeded, the action minerals within the rock continued to dissolve and precipitate. This ultimately led to an increase in the void space of the specimen, a gradual weakening of the bond between the mineral particles, and a deterioration in the mechanical properties.

The red sandstone specimens contained mainly quartz (SiO_2), potassium feldspar (KAlSi_3O_8), sodium feldspar

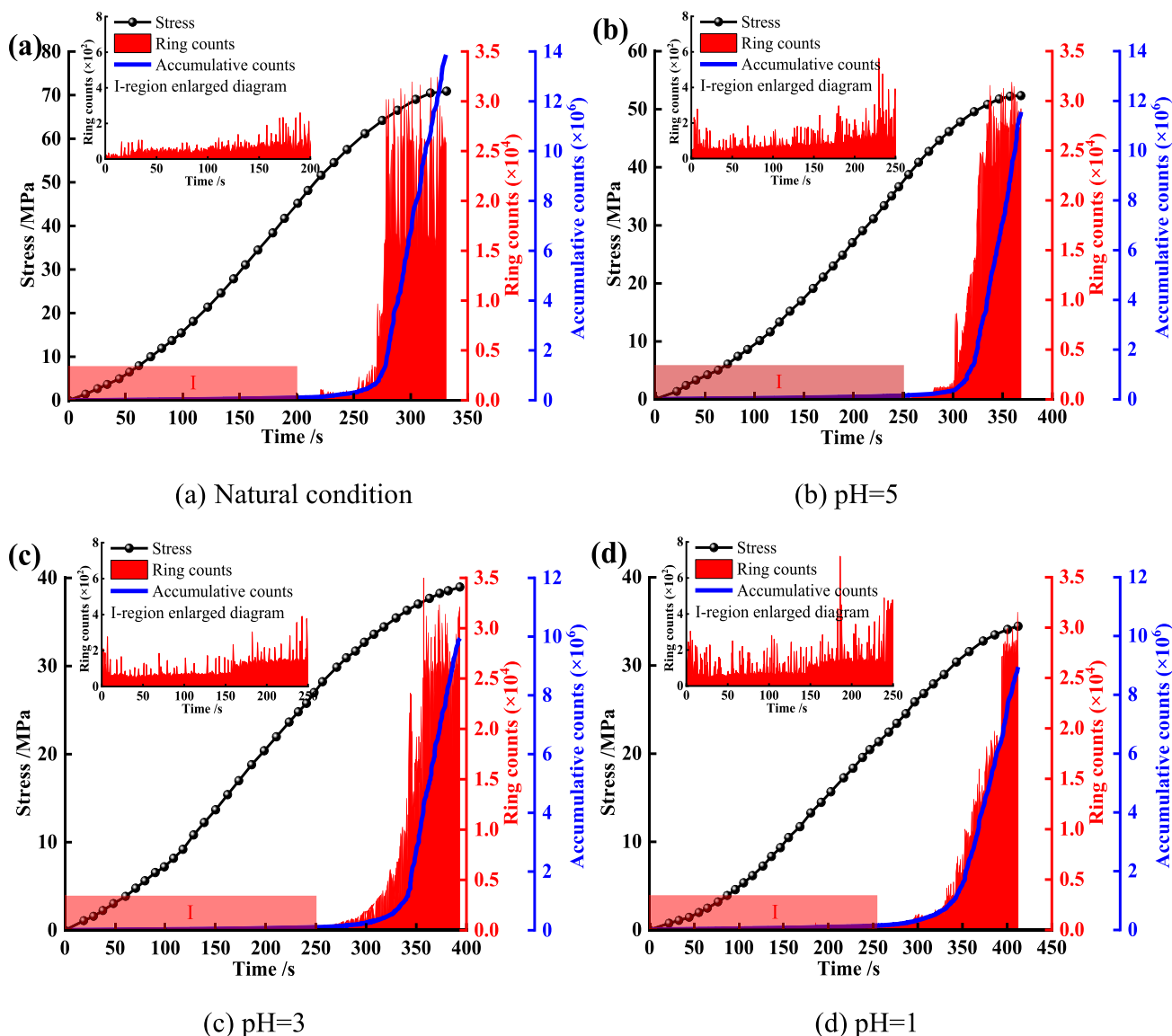
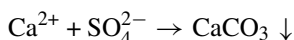
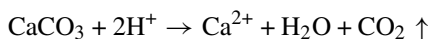
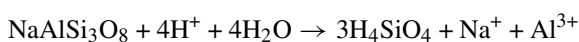
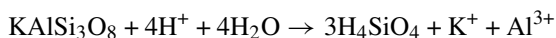


Fig. 6 Variations of acoustic emission ring count (cumulative ring count) of rock specimens under different corrosion conditions

($\text{NaAlSi}_3\text{O}_8$), and calcite (CaCO_3). These ions in the sulfuric acid solution that contained a large amount of H^+ and SO_4^{2-} were involved in the following chemical reactions during the corrosion phase.



The internal microstructure of rock specimens was altered as a result of these chemical reactions that destroyed the rock particles, crystals, and their bonds. From a macroscopic perspective, the compressive strength and elastic modulus of rock specimens decreased while the peak strain increased, indicating a degradation of the mechanical properties. Furthermore, the cumulative AE ringing counts suggested that chemical corrosion also affected the internal structure of the rock specimens, lowering energy required for deformation and raising their plasticity.

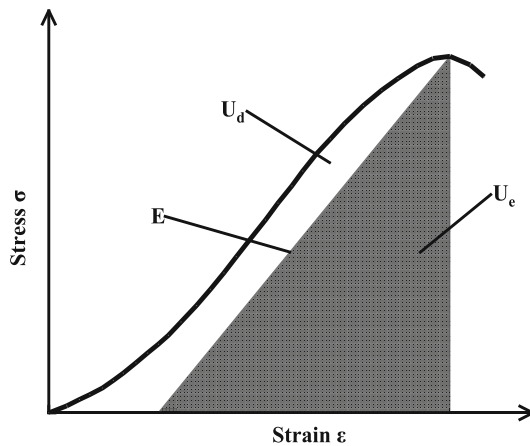


Fig. 7 Relationship between elastic strain energy and dissipated energy of rock specimen

4 Analysis of Energy Evolution of Rock Specimens

4.1 Principle of Energy Calculation

It was assumed that the specimen did not exchange heat with the outside during the loading process, i.e., the specimen was in a closed system. The first law of thermodynamics states that the total input energy generated by the work done on the specimen by the outside is given by

$$U = U^e + U^d \quad (1)$$

where U^d is dissipated energy and U^e is elastic strain energy. The stress–strain relationship curves of the rock specimen and the relationship between dissipated energy U^d and elastic strain energy U^e are displayed in Fig. 7.

The energy of each part of the unit rock is expressed in the principal stress space as

$$U^e = \frac{1}{2}\sigma_1\varepsilon_1^e + \frac{1}{2}\sigma_2\varepsilon_2^e + \frac{1}{2}\sigma_3\varepsilon_3^e \quad (2)$$

where $\sigma_1, \sigma_2, \sigma_3$ are the stresses in the three loading directions; $\varepsilon_1^e, \varepsilon_2^e, \varepsilon_3^e$ are the elastic strains corresponding to the stresses.

Following the Hooke's law:

$$U^e = \frac{1}{2E} \left[\sigma_1^2 + \sigma_2^2 + \sigma_3^2 - 2\nu(\sigma_1\sigma_2 + \sigma_2\sigma_3 + \sigma_1\sigma_3) \right] \quad (3)$$

where E is the initial elastic modulus; ν is the Poisson's ratio. For uniaxial compression test, the calculation formula of the elastic strain energy U^e can be simplified as

$$U^e = \frac{\sigma_1^2}{2E} \quad (4)$$

The total energy U can be calculated as follows:

$$U = \int \sigma_1 d\varepsilon_1 = \sum_{i=1}^{n-1} \int_{\varepsilon_i}^{\varepsilon_{i+1}} \sigma_i d\varepsilon_1 = \sum_{i=1}^{n-1} \frac{\varepsilon_{i+1} - \varepsilon_i}{2} (\sigma_{i+1} + \sigma_i) \quad (5)$$

where σ_i and ε_i are the stress and strain values at each point on the stress–strain curve of rock specimen, respectively. Therefore, the dissipated energy of rock specimen during deformation and destruction process can be obtained as

$$U^d = U - U^e \quad (6)$$

4.2 Energy Evolution Characteristics

The study of the law of energy change in the rock loading process and its relationship with strength and damage is important to understanding how the rock strength changes under loading and the nature of its damage. Total energy, elastic strain energy, and dissipated energy of the specimen during deformation and destruction process under different corrosion conditions were calculated using the formula mentioned above. Since the rock specimens in this study were brittle rocks, the stage after the peak was not well defined. Therefore, this paper focused on the calculation and analysis of energy of rock specimens up to their peaks. The energy change pattern and stress–strain curves of rock specimens under different corrosion conditions are presented in Fig. 8.

Total energy, elastic strain energy, and dissipated energy in the compression stage encountered a gradual increase. Frictional closure caused the microcracks within the specimen to gradually close at the same time. Consequently, the majority of the energy that the rock specimens absorb was transformed into dissipated energy. The stress–strain curve had a small slope because the cracks inside rock specimen were compacted and closed. The area between the stress–strain curves and the coordinate axis can be used to compute total energy. Since the slope was small in the compression stage, the total energy grew slowly. Plastic deformation made up the majority of the deformation in this stage, whereas elastic deformation mostly happened in the elastic stage. Therefore, the elastic strain energy grew slowly during the compression stage. The closure of internal microfractures in the rock specimens was the primary cause of the energy that dissipated during the compression stage. The closure of internal microfractures required less energy than the formation and expansion of cracks in the plastic stage. As a result, the dissipated energy during this stage was small and grew slowly. Toward the end of the compression stage, the dissipated energy growth rate of rock specimens under natural condition started to decrease. However, the dissipated energy growth rate of rock specimens after corroding in the acid solution did not exhibit a decreasing trend. In fact, these



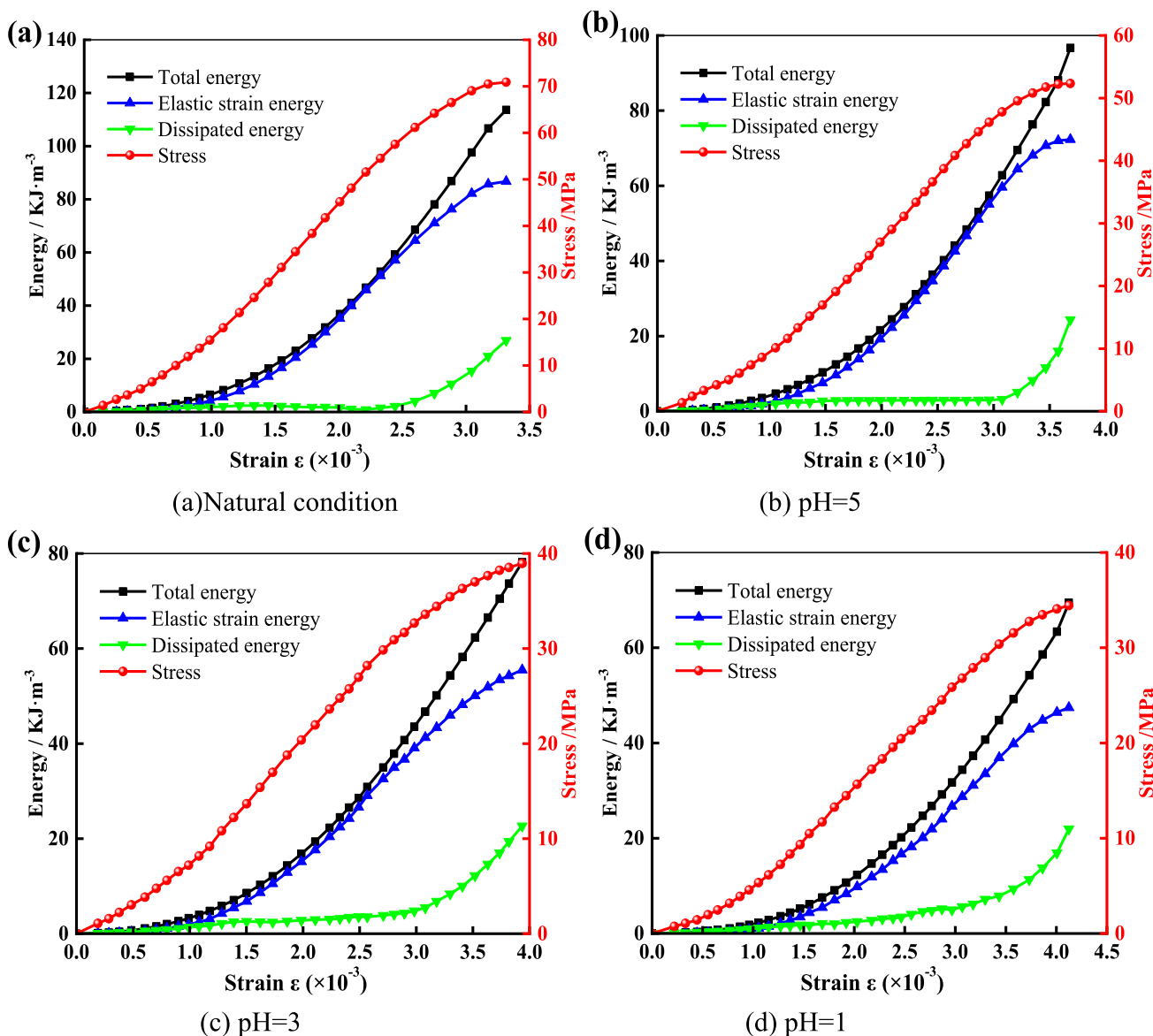


Fig. 8 Energy evolution curves of rock specimens under different corrosion conditions

phenomena became more pronounced as the acidity of the solution increased. This was due to the fact that the integrity of the internal structure of rock specimens in their natural state had been improved after the compression stage. Because of this, there was little increase in dissipated energy during the subsequent elastic stage, with elastic strain energy making up the majority of the total energy. On the other hand, rock specimens maintained under acid solution experienced corrosive effects, leading to the formation of more microdefects and deterioration of the internal structure. These cracks and defects contributed to friction, sliding, and generation of new cracks, resulting in a higher dissipated energy. Consequently, the growth rate of dissipated energy remained unchanged even after the compression stage.

The rock specimen mostly accumulated elastic strain energy during the elastic stage. Under natural conditions, the growth rates of total energy and elastic strain energy initially overlapped and produced overlapping curves. Total energy was predominantly the elastic strain energy, with minimal dissipated energy. However, the curves of total energy and elastic strain energy started to diverge when rock specimens were subjected to acid corrosion in different acid solutions. The degree of separation increased with the acidity of the maintenance solution, and the dissipated energy kept rising steadily during this stage.

Under both natural and acidic solution conditions, the energy evolution trends of rock specimens during the plastic stage were similar. During this stage, the internal cracks

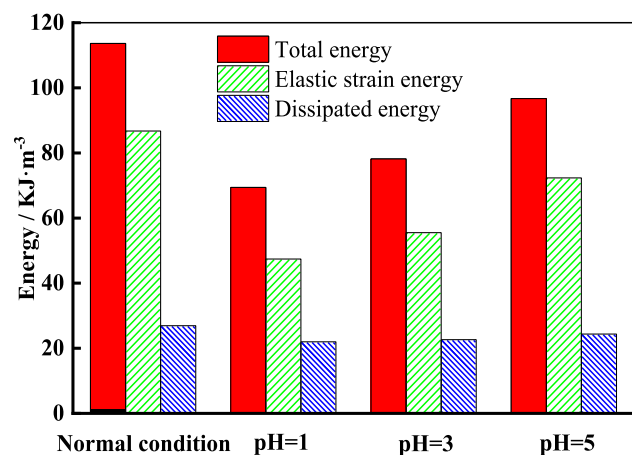


Fig. 9 Relationship between the peaks of each energy of rock specimens under different corrosion conditions

developed and penetrated rapidly, leading to an increase in irreversible plastic deformation and dissipated energy. However, the elastic strain energy increased at a slower rate. As the damage stage approached, the cracks further developed, resulting in the formation of a fracture surface. This was the point at which the elastic strain energy reached its maximum energy storage capacity, leading to a rapid increase in the corresponding dissipated energy and immediate total damage.

4.3 Effect of Corrosive Solutions on Energy Evolution

The relationship between the peaks of each energy of rock specimens under different corrosion conditions is displayed in Fig. 9.

As indicated in Fig. 9, the peak total energy and peak elastic strain energy of the rock specimens under natural condition, pH = 1, pH = 3, and pH = 5 conditions were calculated. Peak total energy values for these conditions were 113.63, 69.40, 78.17, and 96.69, respectively, while the corresponding peak elastic strain energy values were 86.72, 47.43, 55.51, and 72.33. Comparing these values with the uncorroded rock specimens, it was observed that the decrease rates of peak total energy under pH = 1, pH = 3, and pH = 5 acid solution corrosion conditions were 38.92%, 31.21%, and 14.91%, respectively. Similarly, the decrease rates of peak elastic strain energy were 45.31%, 35.99%, and 16.59%, respectively. These results indicated that peak total energy and peak elastic strain energy of rock specimens decreased during the damage caused by acid solution corrosion. Furthermore, the stronger the acidity of the corrosion solution, the greater the decrease. These findings suggested that the mechanical properties of rock specimens corroded by acid solution deteriorated, lowering their capacity to withstand external loads and store energy and increasing the risk of damage.

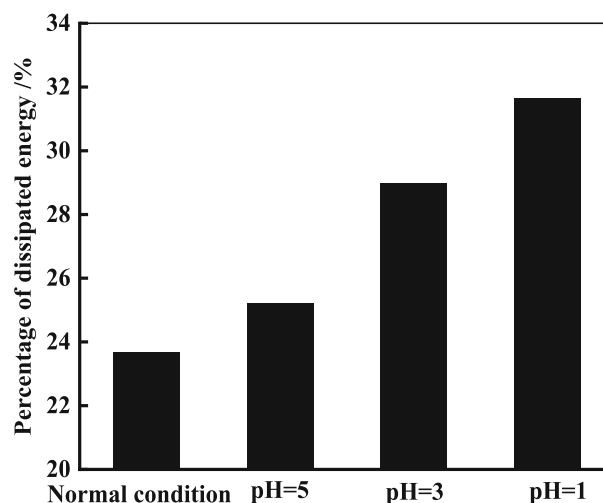


Fig. 10 Percentage of dissipated energy at the moment of rock specimen destruction

The peak elastic strain energy represents the maximum energy storage capacity of the rock specimen. This capacity decreased after acid solution corrosion, which could be attributed to the increased internal damage and the generation of more microcracks in rock specimens. The rock specimens in their natural state demonstrated a restricted capacity for plastic deformation and stored elastic strain energy through elastic deformation. However, after acid corrosion, the internal damage to the rock specimens increased, which raised their capacity for plastic deformation. The elastic strain energy and total energy storage capacity of rock specimens decreased as a result of increased energy consumption by plastic deformation.

To further analyze the impact of pH of the corrosion solution on the rock specimens, the ratio of dissipated energy to total energy during the damage of rock specimens was compared (as indicated in Fig. 10). It was evident that under natural condition, the percentage of dissipated energy during the damage of the rock specimens increased with decreasing pH values of the corrosion solution. Specifically, the percentages for pH values of 5, 3, and 1 were 23.69%, 25.20%, 28.99%, and 31.66%, respectively. As the acidity of the corrosive solution increased, the chemical damage became more severe, leading to a higher percentage of energy dissipation. This observation suggested that a larger percentage of energy absorbed from the external environment was converted into dissipated energy, which caused the rock specimens to be crushed and deformed more severely. Consequently, rock specimens exhibited a higher plastic deformation capacity.

5 Fractal Characteristics of Crushed Rock Specimens

The degree of fragmentation of rock specimens under various corrosion conditions can be quantitatively characterized by the size and mass of rock specimen fragments. This analysis allowed for investigating the distribution characteristics of fragmentation lumpiness. Using different-sized sieves, the collected specimen fragments were classified into eight particle size groups (d represents the particle size) of $0 < d \leq 0.25$ mm, $0.25 < d \leq 0.5$ mm, $0.5 < d \leq 1$ mm, $1 < d \leq 2$ mm, $2 < d \leq 5$ mm, $5 < d \leq 20$ mm, $20 < d \leq 40$ mm, and $40 < d \leq 60$ mm. The mass of broken pieces of each particle size group was measured using an electronic balance. The fragmentation distributions and fragmentation patterns of rock specimens under different corrosion conditions are displayed in Figs. 11 and 12, respectively. The distribution of crushed pieces of rock specimens is listed in Table 3.

Since it is difficult to precisely count the size and number of rock specimen fragments, the fractal dimension was employed to characterize this irregular geometric pattern. It is possible to ascertain the fractal dimension of rock specimen fragmentation by considering the mass–size relationship in the fractal geometry. This analysis contributed to a better understanding of the fragmentation characteristics of rock specimens under different corrosion conditions. The block size distribution of rock specimen fragmentation can be expressed as follows:

$$M_r/M = (r/R)^{3-D} \tag{7}$$

where r and R are the particle size of the fragments and the maximum particle size of the fragments; M_r and M are the cumulative mass of the fragments with particle size less than

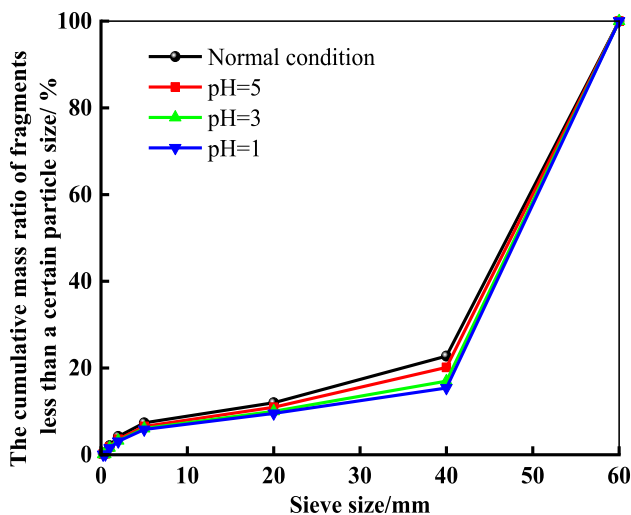


Fig. 11 Fragmentation distributions of rock specimens under different corrosion conditions

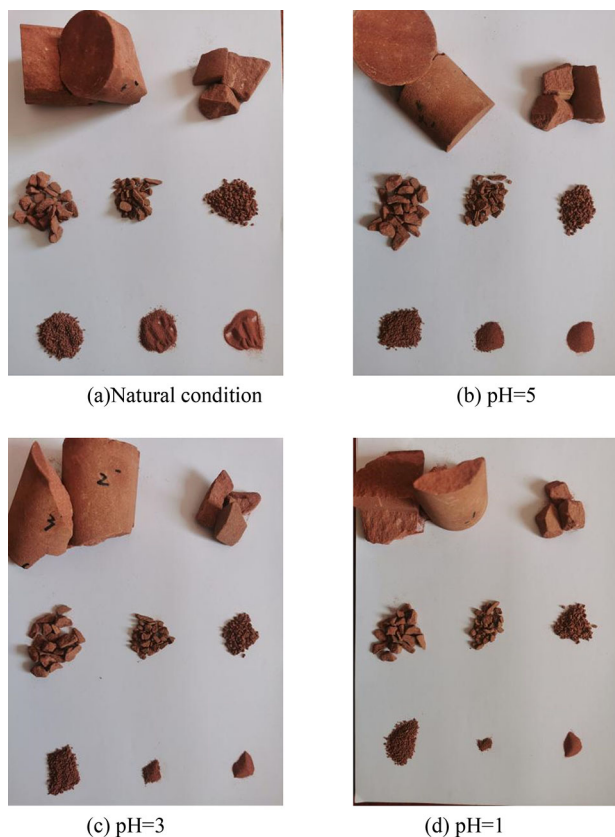


Fig.12 Fragmentation patterns of rock specimens under different corrosion conditions

r and the total mass of the fragments. The formula can be obtained by taking the logarithm on both sides.

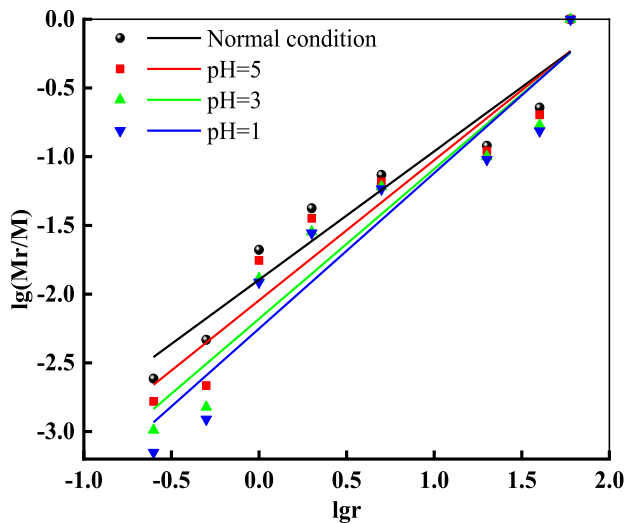
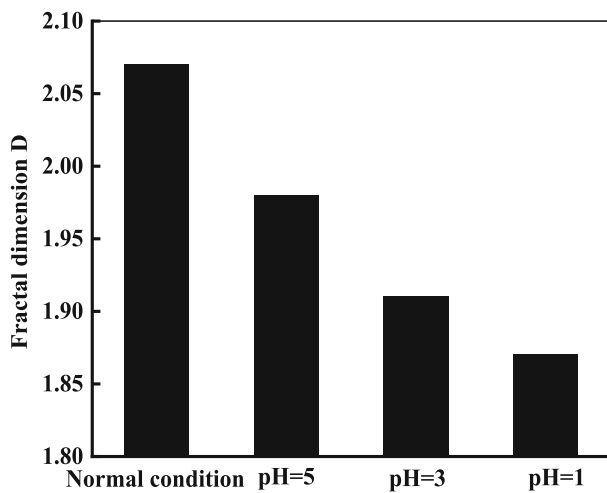
$$\lg(M_r/M) = (3 - D)\lg(r/R) \tag{8}$$

In the linear fitting of each group of data in the $\lg(M_r/M)$ - $\lg r$ double logarithmic coordinate system, the slope of the fitted straight line was $3 - D$, so as to calculate the fractal dimension of the broken fractal of rock specimens under different corrosion conditions, D . The $\lg(M_r/M)$ - $\lg r$ lines of fragment size distributions of rock specimens under different corrosion conditions are displayed in Fig. 13.

The results in Fig. 13 demonstrate a strong correlation between the cumulative sub-sieve mass percentage of a given grain size for each rock specimen and the sieved grain size scatter data in the double logarithmic coordinate system. The correlation coefficients exceeding 0.9 indicated a strong linear relationship. These findings suggested that under different corrosion conditions, the distribution of fractured bulkiness of rock specimens exhibited fractal characteristics. A higher fractal dimension corresponded to a greater number of broken pieces, smaller particle sizes, and higher degree of fragmentation.

Table 3 Distribution of the crushed pieces of the rock specimens under different corrosion conditions

Corrosion conditions	Mass of fragments under the sieve at different grain sizes/g							
	$0 < d \leq 0.25$	$0.25 < d \leq 0.5$	$0.5 < d \leq 1$	$1 < d \leq 2$	$2 < d \leq 5$	$5 < d \leq 20$	$20 < d \leq 40$	$40 < d \leq 60$
Natural	1.15	1.06	7.77	10.07	14.96	22.05	51.16	367.48
pH = 5	0.77	0.23	7.13	8.32	13.75	20.46	42.43	368.93
pH = 3	0.47	0.08	6.79	7.53	12.93	18.15	31.97	380.98
pH = 1	0.32	0.01	6.51	7.02	12.31	16.7	26.3	380.52

**Fig. 13** $\lg(M_r/M)$ - $\lg r$ lines of fragment size distributions of rock specimens under different corrosion conditions**Fig. 14** Relationship between fractal dimension and corrosion conditions

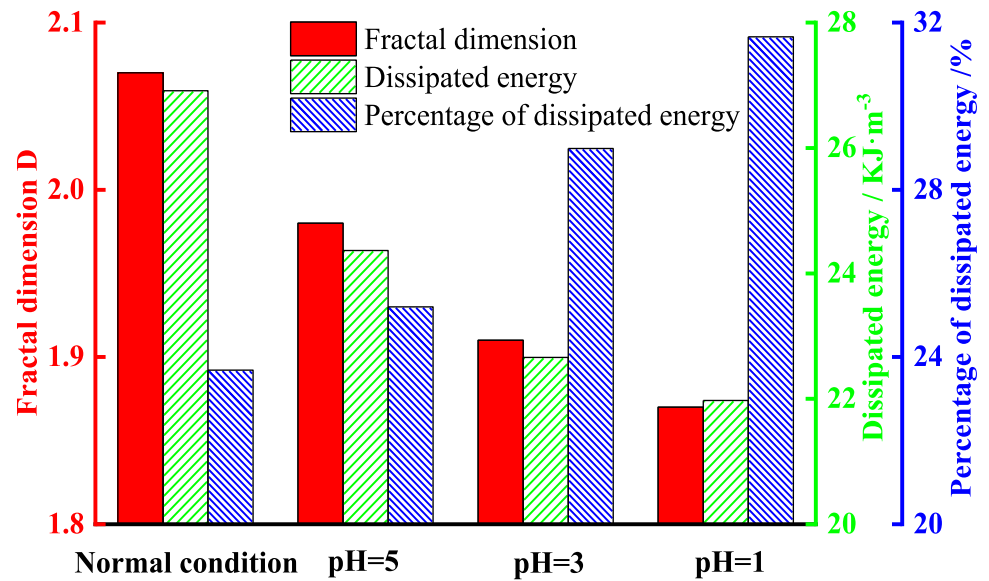
As can be seen in Fig. 14, the fractal dimension of rock specimens decreased as the acidity of the corrosion solution increased. The fractal dimension of broken rock specimens under natural condition and under curing conditions of pH =

5, pH = 3, and pH = 1 was 2.07, 1.98, 1.91, and 1.87, respectively. The fractal dimension of rock specimens under pH = 1 corrosion condition decreased by 9.66% compared with those under natural condition. This provided more evidence that the stronger the acidity of curing solution, the lower the fragmentation of rock specimens.

Furthermore, the acidity of the corrosion solution had a significant effect on the fragmentation pattern of rock specimens. The degree of fragmentation of rock specimens was closely related to their fragmentation dissipated energy. The degree of fragmentation in a rock is gauged by its fractal dimension. A higher fractal dimension indicates a higher degree of fragmentation. When the rock specimen was corroded by an acid solution, the chemical reaction between the solution and the specimen damaged the internal structure of the rock. The degree of damage to rock specimen increased with the acidity of the corrosion solution, leading to an increase in its plastic deformation capacity. During uniaxial compression, the rock specimen experienced greater plastic deformation in the loading direction, resulting in a decrease in both the degree of fragmentation and the fractal dimension. Therefore, in this study, the relationship between the fractal dimension of rock specimen fragmentation and its dissipated energy under different conservation conditions was thoroughly investigated, and the relationship between fractal dimension, dissipated energy and percentage of dissipated energy under corrosion conditions are displayed in Fig. 15.

Figure 15 reveals that as the acidity of the corrosion solution increased, the fractal dimension of rock specimens and the dissipated energy both tended to decrease, while the percentage of dissipated energy tended to increase. The nature of rock deformation and destruction involved the input, storage, and release of energy under load, with the fractal dimension representing the degree of rock fragmentation. Rock specimens under natural conditions had higher strength and less deformation before damage than corroded rock specimens. They also had larger total energy and dissipated energy before destruction. However, as plastic deformation could only release a limited amount of energy, rapid expansion occurred when the stored energy reached its limit, leading to destruction. The rock specimens now dissipated a significant

Fig. 15 Relationship between fractal dimension, dissipated energy and percentage of dissipated energy under corrosion conditions



amount of energy, resulting in a more violent crushing and a higher corresponding fractal dimension. Rock specimens corroded by an acidic solution suffered internal structural damage that reduces strength, increases deformation, and decreases total energy and dissipated energy before destruction. The energy released by plastic deformation increased after corrosion, with a higher percentage of dissipated energy. These resulted in a decrease in the degree of fragmentation and the corresponding fractal dimension.

6 Conclusions

1. The peak strain and plastic deformation capacity of rock specimens increased, while their compressive strength and elastic modulus decreased after being corroded by an acid solution. In addition, the cumulative AE ringing count decreased, and the duration of the high-level AE ringing was shortened. These resulted from a physico-chemical reaction between the mineral composition of rock specimens and the acid solution, which caused continuous dissolution and precipitation of the minerals within the rock. Consequently, the bond between the mineral particles gradually weakened, resulting in deterioration of the mechanical properties.
2. Prior to reaching the plastic stage, the rates of energy dissipation of corroded rock specimens were higher than those of uncorroded rock specimens. This was due to the quick development of internal losses in rock specimens corroded by the acid solution. In comparison with the uncorroded rock specimens, the corroded rock specimens had less damage during the plastic stage. The

dissipated energy decreased but the percentage of dissipated energy increased as the acidity of the corrosion solution increased.

3. Peak total energy and peak elastic strain energy of rock specimens decreased as the acidity of the corrosion solution increased, which resulted in an increase in the deterioration of the internal structure. In addition, both the energy absorption capacity and the energy storage limit of rock specimens decreased with the increasing corrosion.
4. The acidity of the corrosion solution had a significant impact on the fragmentation pattern and fractal dimension of rock specimens. The fractal dimension of fragmentation and the dissipated energy of rock specimens decreased as the acidity of the corrosion solution increased. The fractal dimension of rock specimens under $\text{pH} = 1$ corrosion condition decreased by 9.66% compared to the uncorroded rock specimens. This finding provided more evidence in favor of the hypothesis that reduced rock specimen fragmentation was caused by a higher acidity of the corrosion solution.

Acknowledgments The project presented in this article is supported by the Open Fund Project of State Key Laboratory of Mining Response and Disaster Prevention and Control in Deep Coal Mines, China (Grant no. SKLMRDPC22KF14) and the Science and Technology Project of Jiangxi Provincial Department of Education, China (Grant nos. GJJ2207301 and GJJ2207306).

Data availability The datasets generated during and/or analyzed during the current study are available from the corresponding author on reasonable request.

Declarations

Conflict of interest This study has no conflict of interest.

References

- Park, S.; Kim, J.S.; Kwon, S.: Investigation of the development of an excavation damaged zone and its influence on the mechanical behaviors of a blasted tunnel. *Geosyst. Eng.* **21**(3), 165–181 (2018). <https://doi.org/10.1080/12269328.2018.1461139>
- Yang, Y.; Jiang, Q.; Liu, J.; Zheng, H.; Xu, D.P.; Xiong, J.: Equivalent constitutive model for jointed rock masses and its application in large underground caverns. *Int. J. Geomech.* **23**(1), 04022259 (2023). <https://doi.org/10.1007/s40999-023-00899-1>
- Zhang, Y.; Chen, C.H.; Gao, S.F.; Guo, S.Q.; Li, N.; Hu, Z.Q.; Yang, S.S.: A novel binary-medium breakage model for loess in an acidic aqueous environment. *Bull. Eng. Geol. Environ.* **82**, 210 (2023). <https://doi.org/10.1007/s10064-023-03227-y>
- Chen, Y.L.; Chen, Q.J.; Pan, Y.G.; Xiao, P.; Du, X.; Wang, S.R.; Zhang, N.; Wu, X.J.: A chemical damage creep model of rock considering the influence of triaxial stress. *Mater* **15**, 7590 (2022). <https://doi.org/10.3390/ma15217590>
- Chen, Y.L.; Xiao, P.; Du, X.; Wang, S.R.; Wang, Z.L.; Azzam, R.: Study on damage statistical constitutive model of triaxial compression of acid-etched rock under coupling effect of temperature and confining pressure. *Mater* **14**, 7414 (2021). <https://doi.org/10.3390/ma14237414>
- Zhang, H.D.; Doi, S.Y.; Zhao, G.C.; Yang, H.Q.; Wu, C.Y.: Study on complex theory solution and numerical simulation of fracture mechanics of surrounding rock stress and energy field in fault type rock burst stope. *Adv. Mater. Sci. Eng.* **2022**, 6909248 (2022). <https://doi.org/10.1155/2022/6909248>
- Pan, J.L.; Ren, F.H.; Cai, M.F.: Effect of joint density on rockburst proneness of the elastic-brittle-plastic rock mass. *Shock. Vib.* **2021**, 5574325 (2021). <https://doi.org/10.1155/2021/5574325>
- Huang, B.X.; Hou, M.X.; Zhao, X.L.; Ying, Y.K.: Experimental investigation on the reformation and strength weakening of hard limestone by acidizing. *Int. J. Min. Sci. Technol.* **32**, 965–979 (2022). <https://doi.org/10.1016/j.ijmst.2022.08.008>
- Cao, X.X.; Feng, M.M.; Yuan, K.S.: Dynamic mechanical properties and damage mechanism of freeze-thaw sandstone under acid corrosion. *Geofluids* **2021**, 7335284 (2021). <https://doi.org/10.1155/2021/7335284>
- Chen, Q.J.; Chen, Y.L.; Xiao, P.; Du, X.; Pan, Y.G.; Azzam, R.: Mechanical properties and damage constitutive model of sandstone after acid corrosion and high temperature treatments. *Int. J. Min. Sci. Technol.* **33**, 747–760 (2023). <https://doi.org/10.1016/j.ijmst.2022.11.011>
- Li, S.G.; Huo, R.K.; Wang, B.; Ren, Z.Z.; Ding, Y.; Qian, M.T.; Qiu, T.: Experimental study on physicochemical properties of sandstone under acidic environment. *Adv. Civ. Eng.* **2018**, 5784831 (2018). <https://doi.org/10.1155/2018/5784831>
- Huo, R.K.; Li, S.G.; Han, F.; Wang, G.J.: CT analysis on mesoscopic structure of sandstone under acidic environment. *Indian J. Geo-Mar. Sci.* **47**(5), 962–971 (2018)
- Huo, R.K.; Qiu, T.; Liang, Y.L.; Li, S.G.; Qian, M.T.: The physicochemical deterioration characteristics and mesoscopic damage analysis of sandstone under acidic environment. *Adv. Civ. Eng.* **2020**, 7467608 (2020). <https://doi.org/10.1155/2020/7467608>
- Bai, B.; Chen, J.; Bai, F.; Nie, Q.K.; Jia, X.G.: Corrosion effect of acid/alkali on cementitious red mud-fly ash materials containing heavy metal residues. *Environ. Technol. Innov.* **33**, 103485 (2023). <https://doi.org/10.1016/j.eti.2023.103485>
- Zhang, S.R.; Bai, X.Y.; Zhao, C.W.; Tan, Q.; Luo, G.J.; Wang, J.F.; Li, Q.; Wu, L.H.; Chen, F.; Li, C.J.; Deng, Y.H.; Yang, Y.J.; Xi, H.P.: Global CO₂ consumption by silicate rock chemical weathering: its past and future. *Earths Future* **9**(5), e2020EF001938 (2021). <https://doi.org/10.1029/2020EF001938>
- Luo, S.; Gong, F.Q.: Linear energy storage and dissipation laws during rock fracture under three-point flexural loading. *Eng. Fract. Mech.* **234**, 107102 (2020). <https://doi.org/10.1016/j.engfracmech.2020.107102>
- Luo, S.; Gong, F.Q.; Li, L.L.; Peng, K.: Linear energy storage and dissipation laws and damage evolution characteristics of rock under triaxial cyclic compression with different confining pressures. *Trans. Nonferrous Met. Soc. China* **33**, 2168–2182 (2023). [https://doi.org/10.1016/S1003-6326\(23\)66251-X](https://doi.org/10.1016/S1003-6326(23)66251-X)
- Yu, Y.; Zhao, D.C.; Feng, G.L.; Geng, D.X.; Guo, H.S.: Energy evolution and acoustic emission characteristics of uniaxial compression failure of anchored layered sandstone. *Front. Earth Sci.* **10**, 841598 (2022). <https://doi.org/10.3389/feart.2022.841598>
- Yu, Y.; Feng, G.L.; Xu, C.J.; Chen, B.R.; Geng, D.X.; Zhu, B.T.: Quantitative threshold of energy fractal dimension for immediate rock-burst warning in deep tunnel: a case study. *Lithosphere* (2022). <https://doi.org/10.2113/2022/1699273>
- Wu, W.X.; Gong, F.Q.: Investigation on energy evolution and storage characteristic of cstbd red sandstone during mixed-mode fracture. *Geofluids* **2022**, 9822469 (2022). <https://doi.org/10.1155/2022/9822469>
- Meng, Q.B.; Liu, J.F.; Huang, B.X.; Pu, H.; Wu, J.Y.; Zhang, Z.Z.: Effects of confining pressure and temperature on the energy evolution of rocks under triaxial cyclic loading and unloading conditions. *Rock Mech. Rock Eng.* **55**, 773–798 (2022). <https://doi.org/10.1007/s00603-021-02690-x>
- Yang, R.S.; Li, W.Y.; Yue, Z.W.: Comparative study on dynamic mechanical properties and energy dissipation of rocks under impact loads. *Shock. Vib.* **2020**, 8865099 (2020). <https://doi.org/10.1155/2020/8865099>
- Gong, F.Q.; Hu, J.: Energy dissipation characteristic of red sandstone in the dynamic brazilian disc test with shpb setup. *Adv. Civ. Eng.* **2020**, 7160937 (2020). <https://doi.org/10.1155/2020/7160937>
- Li, M.X.; Song, Y.H.; Zhang, G.: Study on the fractal characteristics of rock in the prediction of rockburst. *RSC Adv.* **7**, 43073–43082 (2017). <https://doi.org/10.1039/c7ra03947f>
- Zhu, S.Y.; Wu, Y.; Lu, L.L.: Fragmentation evolution and fractal characteristics of deep rocks by lab compression-shear tests. *J. Test. Eval.* **46**(4), 1548–1558 (2018). <https://doi.org/10.1520/JTE20160491>
- Li, Y.Y.; Zhang, S.C.; Zhang, X.: Zhang X (2018) Classification and fractal characteristics of coal rock fragments under uniaxial cyclic loading conditions. *Arab. J. Geosci.* **11**, 201 (2018). <https://doi.org/10.1007/s12517-018-3534-2>
- Wang, J.G.; Zuo, T.; Li, X.L.; Tao, Z.H.; Ma, J.: Study on the fractal characteristics of the pomegranate biotite schist under impact loading. *Geofluids* **2021**, 1570160 (2021). <https://doi.org/10.1155/2021/1570160>
- Chai, Z.Y.; Bai, J.B.; Zhang, H.Y.; Yang, P.: Evolution rules of fractures for mudstone under compression shear load and the fractal characteristics of broken blocks. *Adv. Civ. Eng.* **2019**, 2489218 (2019). <https://doi.org/10.1155/2019/2489218>
- Tian, B.Z.; Liu, S.J.; Zhang, Y.B.; Wang, Z.L.: Analysis of fractal characteristic of fragments from rock burst tests under different loading rates. *Tehnički vjesnik* **23**(5), 1269–1276 (2016). <https://doi.org/10.17559/TV-20160815152017>

Springer Nature or its licensor (e.g. a society or other partner) holds exclusive rights to this article under a publishing agreement with the author(s) or other rightsholder(s); author self-archiving of the accepted manuscript version of this article is solely governed by the terms of such publishing agreement and applicable law.